THE ASTROPHYSICAL JOURNAL, 557:659–670, 2001 August 20

VERY LARGE ARRAY OBSERVATIONS OF THE H92α LINE FROM NGC 5253 AND HENIZE 2-10: IONIZED GAS AROUND SUPER STAR CLUSTERS

NIRUJ R. MOHAN
Raman Research Institute, CV Raman Avenue, Sadashivanagar Post Office, Bangalore 560-080, India; and Indian Institute of Science, Joint Astronomy Program, Bangalore 560 012, India; niruj@rri.res.in

K. R. ANANTHARAMAIAH
Raman Research Institute, CV Raman Avenue, Sadashivanagar Post Office, Bangalore 560-080, India; anantha@rri.res.in

AND

W. M. GOSS
National Radio Astronomy Observatory, P.O. Box O, Socorro, NM 87801; mgoss@aoc.nrao.edu
Received 2001 April 4; accepted 2001 April 24

ABSTRACT

We have detected the H92α radio recombination line from two dwarf starburst galaxies, NGC 5253 and He 2-10, using the Very Large Array. Both the line data as well as the radio continuum data are used to model the properties of the ionized gas in the centers of these galaxies. We consider a multi-density model for radio recombination lines and show why previous models, which were based on the assumption of gas at a single density, are valid in many situations. The models show that the ionized gas has a density of $\sim 10^4$ cm^{-3} in both galaxies, with an effective size of 2–10 pc and a total mass of $\sim 10^4$ $M_\odot$. The derived production rate of Lyman continuum photons is $\sim 2.5 \times 10^{52}$ s^{-1} in both the galaxies, and the corresponding mass of stars (assuming a Salpeter initial mass function) is $\sim 10^5$ $M_\odot$. The implied stellar density shows that the observed radio recombination lines arise from ionized gas around super star clusters (SSCs) in both galaxies (these SSCs have been recently detected through their radio continuum emission). The existence of $\sim 10^4$ $M_\odot$ of ionized gas within a few parsecs of an SSC places strict constraints on dynamical models. Using simple arguments, the parameter space for a few possible models are derived. The well-known radio–far-infrared correlation also holds for NGC 5253, although the radio emission from this galaxy is almost completely thermal. It is shown that NGC 5253 is strong evidence that the component of far-infrared emission from warm dust is correlated separately with the component of radio emission from thermal bremsstrahlung.

Subject headings: galaxies: individual (Henize 2-10, NGC 5253) — galaxies: ISM — galaxies: starburst — radio lines: galaxies

1. INTRODUCTION

It is now known that star formation in starburst galaxies is not just a scaled-up version of quiescent star formation in normal galaxies. For example, the phenomenon of starbursts involves the formation of super star clusters (SSCs), which are believed to be the precursors of the present-day globular clusters (see the recent review by Whitmore 2000 and references therein). These SSCs may generate large-scale superwind outflows (Heckman, Armus, & Miley 1990) that can carry away a good fraction of the gas and processed heavy elements from the starburst region. Star formation also occurs in the form of individual field stars and small unresolved clusters. Along with stellar emission diagnostics, studies of ionized gas around OB stars provide information on the young stellar population and also characterize the surrounding interstellar medium. Radio continuum and recombination line emissions are good extinction-free probes of this gas. High-resolution radio continuum imaging of starburst centers, for example, has led to the discovery of a host of parsec-sized thermal and nonthermal compact sources (NGC 253: Ulvestad & Antonucci 1997 and references therein; NGC 2146: Tarchi et al. 2000; M82: Kronberg, Biermann, & Schwab 1985; NGC 4038/9: Neff & Ulvestad 2000). Studying the compact thermal sources is difficult in the UV, optical, or even in IR, owing to extinction problems. A nebular diagnostic like radio recombination lines (RRLs) can probe thermal gas with large emission measures (EMs). In the centimeter-wavelength range, RRLs have been shown to be detectable from nuclear starburst regions in a number of nearby galaxies (Shaver, Churchwell, & Rots 1977; Seaquist & Bell 1977; Puxley et al. 1991; Anantharamaiah et al. 1993; Zhao et al. 1996; Phookun, Anantharamaiah, & Goss 1998). These lines have proven to be good probes of gas density and are reliable estimators of ionized gas mass and the ionizing photon flux in these starburst regions. RRLs have been studied in about 14 galaxies so far (Anantharamaiah et al. 2000 and references therein). In this paper we present observations of the H92α RRL at 8.3 GHz from two prototypical blue compact dwarf galaxies (BCDGs), NGC 5253 and He 2-10.

BCDGs are dwarf galaxies that are dominated by an ongoing starburst, with or without background quiescent star formation. NGC 5253 and He 2-10 are classic examples (Davies, Sugai, & Ward 1998) of BCDGs. NGC 5253 ($D = 4.1$ Mpc; Saha et al. 1995) is a dwarf galaxy with an underlying elliptical structure (Caldwell & Phillips 1989). This galaxy has large-scale ionized filaments (Graham 1981) and a number of young star clusters in the halo (van den Bergh 1980). The central kiloparsec region is undergoing active star formation and hosts a number of SSCs (Turner, Beck, & Ho 2000, hereafter TBH00; Calzetti et al. 1997, hereafter CMB97; Gorjian 1996; Beck et al. 1996; Meurer et al. 1995; Caldwell & Phillips 1989). Wolf-Rayet emission

has been detected in the central region (Campbell, Terlevich, & Melnick 1986; Walsh & Roy 1987, 1989; Schaerer et al. 1997). Based on modeling of the stellar emission and through the presence of ambient ionized gas and Wolf-Rayet features (Gorjian 1996), a spatial age gradient in the star formation in the core has been inferred. NGC 5253 is notable for having a flat radio continuum spectrum (Lequeux 1971; Beck et al. 1996), which is attributed to lack of nonthermal radiation due to the absence of supernova remnants (SNRs). This absence is believed to be due to the very young age of the star formation activity. The resulting age estimate is consistent with that derived from optical and IR spectrophotometry (Beck et al. 1996). The Hα structure in the inner 20″ is complex, and there is evidence for a patchy dust distribution (CMB97). Recently, TBH00 have made a high-resolution image of the central region in the radio continuum at 15 and 22 GHz and have detected a compact source that they interpret as a "supernebula" surrounding a nascent SSC.

He 2-10 ($D = 9$ Mpc) was the first Wolf-Rayet galaxy discovered (Allen, Wright, & Goss 1976). Three star-forming regions have been identified in the central part of the galaxy, and among them, the central $\sim 5''$ region, called region "A," is the youngest (Méndez et al. 1999). This region exhibits predominant Wolf-Rayet spectral features and is also the most active star-forming region. *Hubble Space Telescope* (*HST*) imaging in the UV has shown the presence of a series of young clusters, believed to be SSCs (Conti & Vacca 1994; Johnson et al. 2000). Deep Hα images of this galaxy (Méndez et al. 1999) indicate a large-scale bipolar outflow of gas. Molecular gas, imaged through CO lines, shows a disturbed morphology with a rotating disk or a bar (Kobulnicky et al. 1995). Radio continuum from He 2-10 has an overall spectral index of -0.6 and is therefore dominated by nonthermal emission (Allen et al. 1976). Recent high-resolution radio continuum imaging by Kobulnicky & Johnson (1999, hereafter KJ99) has shown the existence of five compact radio knots with flat spectra. These radio knots are interpreted by the authors as high-density nebulae surrounding young SSCs, which are probably totally obscured in the optical.

Based on their nuclear Brγ flux densities and the presence of active star formation in the central region, we selected these two galaxies to search for RRLs from the central few hundred parsecs. Our observations are a part of a program that we have undertaken to detect RRLs in nearby starbursts and to follow up the detected sources using multifrequency RRL and continuum observations. The aim is to model the density structure, kinematics, and geometry of the ionized gas in these regions and to determine an extinction-independent star formation rate. An example of such a study of Arp 220 has been presented by Anantharamaiah et al. (2000).

2. OBSERVATIONS AND RESULTS

NGC 5253 and He 2-10 were observed with the Very Large Array (VLA) in both the CnB and the DnC configurations with an on-source integration time of 3 hr per source in each configuration. Some details of the observations are given in Table 1. The system was tuned to detect the H92α line ($\nu_{\rm rest} = 8309.385$ MHz) using a total bandwidth of 25 MHz and 15 spectral channels. Data from both polarization channels were recorded. The data was Hanning smoothed off line to reduce the effects of Gibbs ringing. The effective velocity resolution is 113 km s^{-1}. The flux density scale was fixed by using 3C 286 as a calibrator, and phase and bandpass calibrations were done by using a nearby point source. All the data analysis was done by using standard algorithms within the software AIPS. The continuum visibility data was self-calibrated and the resultant antenna gains were applied to the line data as well. The CnB and DnC array data of each galaxy were later concatenated, and combined (C+D) continuum and line data sets (with a resolution of $\sim 5''$) were obtained. The final line images were derived after subtracting the continuum using the AIPS task UVLIN, which subtracts a linear function of frequency from the real and imaginary parts of the observed visibilities (Cornwell, Uson, & Haddad 1992). The continuum and line data are presented in Table 2. Figure 1 shows the continuum images of the two galaxies. The images show evidence for filaments, especially in the case of NGC 5253, where there are extensions in the southern direction. These filaments are also seen in optical line and optical continuum images and extend out to a few arcminutes. The total continuum flux density of NGC 5253 at 8.3 GHz is 58 mJy. The radio spectrum of this galaxy is known to be flat from 1.4 up to 23 GHz, based on both single-dish and scaled array VLA observations (see Lequeux 1971 and also Turner, Ho, & Beck 1998 and references therein). Lower resolution images indicate that there is emission over at least 2′. The shortest spacing available in the D configuration of the VLA implies that our images are not sensitive to structures on scales larger than $\sim 2'$. We estimate that the total flux density of NGC 5253 in our image is 80% of the single-dish flux density at 8.3 GHz. The radio continuum emission in NGC 5253 peaks around region "A" (the centimeter-emission peak in Turner et al. 1998), which contains the two main star-forming regions—clusters 4 and 5 (CMB97). The radio continuum emission is weak to the south of the peak, where the older clusters are believed to have dispersed the gas. The radio emission in He 2-10 covers the two main star-forming regions—A and B (region A is the central 6″ region and region B is the secondary star-forming region 8.″5 east of A; Corbin, Korista, & Vacca 1993). Figure 2 shows the H92α-line spectra of the two galaxies at the position of the peak continuum emission. The line emission in both the galaxies

TABLE 1

LOG OF VLA OBSERVATIONS

Galaxy	Array	Date of Observation	UV Range (kλ)	Phase Calibrator	Bandpass Calibrator	$V_{\rm hel}$ (km s^{-1})
NGC 5253.....	DnC	1999 Feb 19	0.7–42	1334-127	1334-127	404
NGC 5253.....	CnB	1998 Nov 10	1.3–150	1334-127	1334-127	404
He 2-10	DnC	1999 Feb 19	0.7–46	0919-260	0919-260	873
He 2-10	CnB	1998 Nov 10	2.0–130	0919-260	0919-260	873

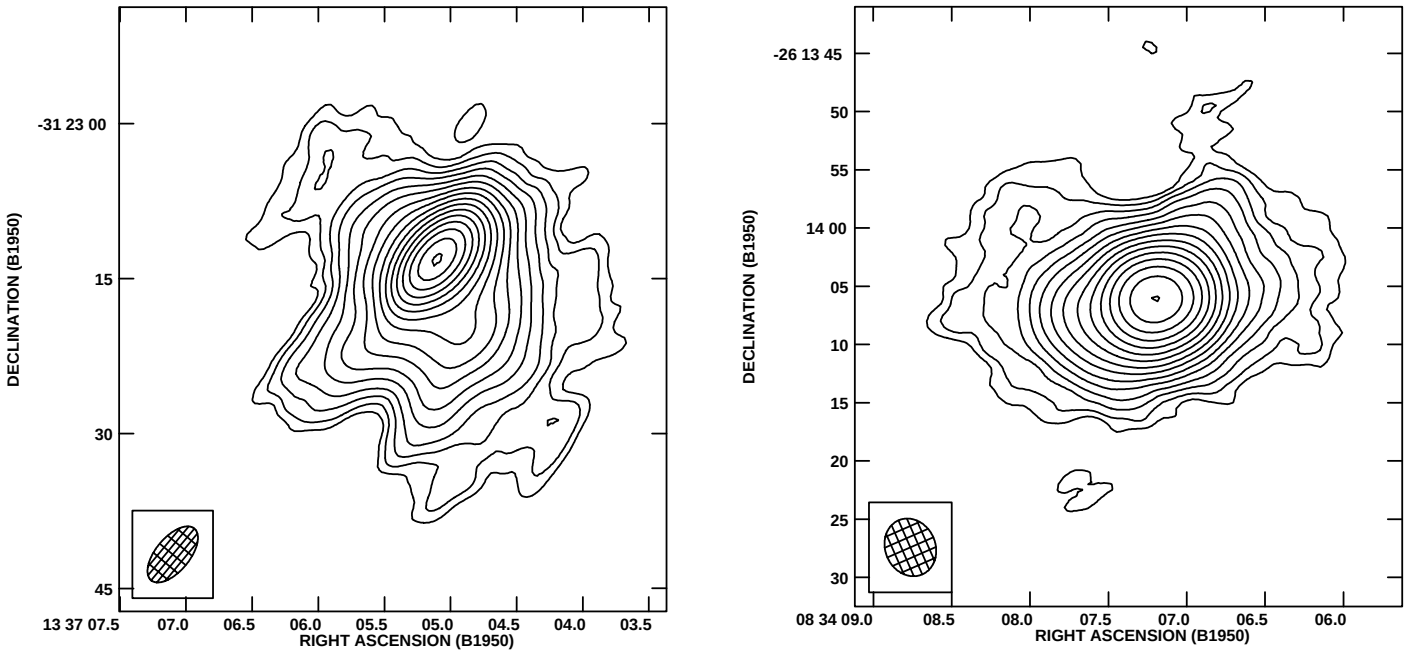

FIG. 1.—The 8.3 GHz radio continuum images of NGC 5253 (*left*) and He 2-10 (*right*) observed using the combined C and D array VLA data, made with "natural weighting" of the visibilities. The contours start at 5 σ (150 and 160 μJy for NGC 5253 and He 2-10, respectively) and increase in steps of $\sqrt{2}$. The beam sizes are 6.″5 × 3.″3, P.A. = −40° for NGC 5253 and 5.″0 × 4.″3, P.A. = 24° for He 2-10. For further details, see Table 2.

is spatially unresolved, even in the higher resolution C-array data. The FWHM of the lines measured on the data sets to which off-line Hanning smoothing was not applied are quoted in Table 2. The FWHM of the H92α line in NGC 5253 agrees well with the value of 105 km s^{-1} estimated from the Hα spectrum of the central 1.″9 region (Atherton et al. 1982).

3. MODELING THE H92α LINE

In this section, we model the observed data in terms of the local electron density, temperature, and size of the ionized gas. The models for the ionized gas are based on the observed H92α-line flux density and the continuum flux densities at 8.3, 4.8, and 15 GHz (see Table 2) from the region of RRL emission. Since the line formation process is dependent on the geometry of the emitting gas, we consider four different models. Model I is for a single spherical H II region of fixed size and constant density. Model II consists of a uniform slab of constant density and fixed thickness and beam filling factor. Model III consists of a collection of H II regions of fixed density and size. The number of such H II regions is normalized using the observed line flux density. The third model is similar to those described by Anantharamaiah et al. (1993) and further adapted by Zhao et al. (1996) and Phookun et al. (1998) for modeling RRLs from ionized gas in starburst regions. For all three models, a parameter search is done in density n_e in the range 10^{-2} cm^{-3} $< n_e < 10^6$ cm^{-3} and size l in the range 0.01 pc $< l < L$ pc, where L is the upper limit to the size of the line-emitting region given by the beam size, which is 150 pc

TABLE 2

OBSERVATIONAL DATA

Parameter	NGC 5253	He 2-10
Beam size (arcsec)	6.5 × 3.3	5.0 × 4.3
P.A. of the beam (deg)	−40	24
Peak continuum flux density at 8.3 GHz (mJy)[a]	28	13
Total continuum flux density at 8.3 GHz (mJy)[b]	58	29
Noise in continuum image (1 σ) (μJy)	27	21
Peak H92α-line flux density[c]	0.53	0.16
Line width (FWHM) before Hanning smoothing (km s^{-1})	95 ± 10	112 ± 20
Noise in channel image (1 σ) (μJy)	65	45
4.8 GHz flux density (mJy)	30[d]	18[e]
15 GHz flux density (mJy)	26[d]	9[e]

[a] Peak continuum flux density in the central 5″ region.

[b] Total continuum flux density measured over the entire C+D continuum image of 30″–45″ extent: 80% of the single-dish flux density (see § 2).

[c] Line flux density in the central beam area of 5″.

[d] Continuum flux density for the central 5″; Turner et al. 1998.

[e] Continuum flux density for the central 5″, assuming $S_\nu \propto \nu^{-0.6}$; see Kobulnicky & Johnson 1999 for a summary of the spectral index of He 2-10.

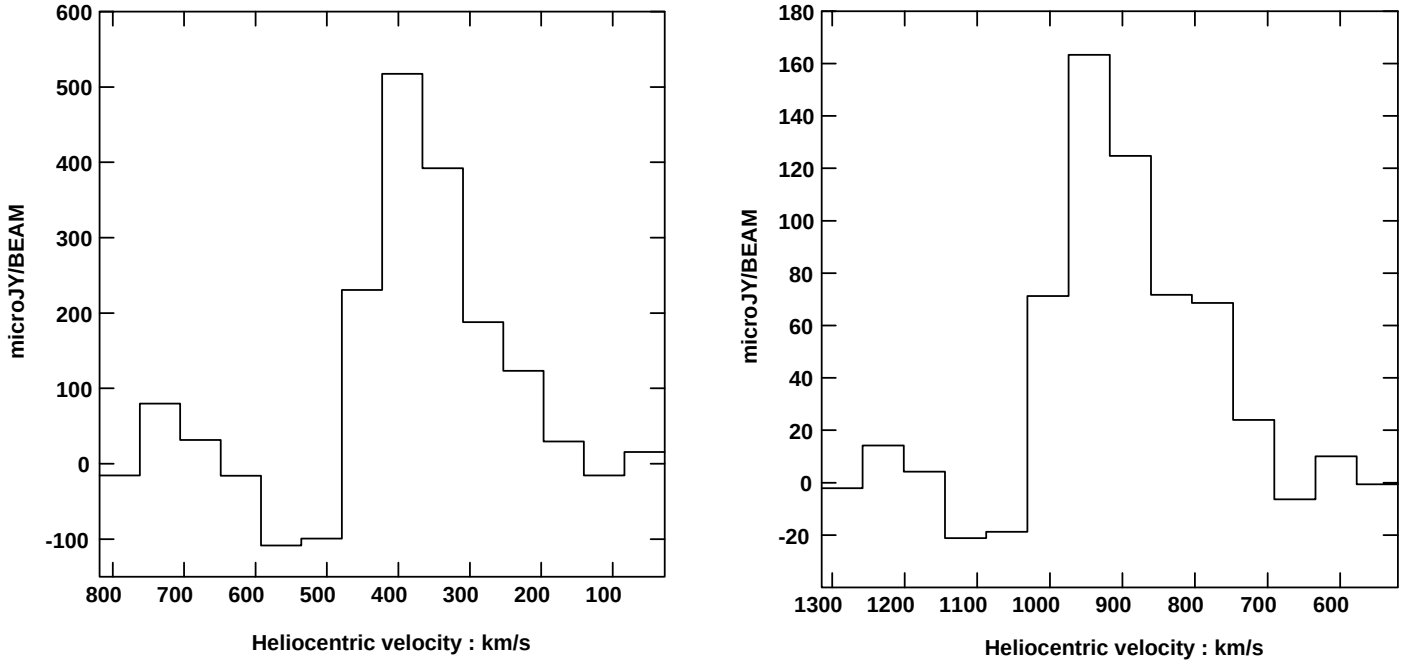

FIG. 2.—Hanning smoothed H92α spectra at the continuum peaks of NGC 5253 (*left*) and He 2-10 (*right*) at 8.3 GHz for the combined C and D array VLA data. The line emission is unresolved in both galaxies. The spatial resolution is 6.″5 × 3.″3 for NGC 5253 and 5.″0 × 4.″3 for He 2-10. The velocity resolution of the spectrum is 113 km s^{-1}.

for NGC 5253 and 315 pc for He 2-10. Model II also includes the beam filling factor as a free parameter, which is the lateral extent of the slab of ionized gas within the region of total lateral size L pc. We also consider a fourth model (Model IV) in which the coexistence of multiple densities is assumed. In this model, we assume a population of H II regions with different densities, but with each H II region having a constant density. We consider those densities that correspond to compact ($n_e > 10^3$ cm^{-3} and diameter d between 0.1 and 1 pc) and ultracompact H II regions ($n_e > 10^4$ cm^{-3} and $d < 0.1$ pc). An H II region of density n_e is assigned a size l given by the relation $n_e = c_1 l^{\alpha}$. The parameters α and c_1 depend on the ambient medium and the evolutionary phase of the H II region. In our model, these are free parameters. There is evidence for the existence of such a power law for galactic compact and ultracompact H II regions (see, for example, Habing & Israel 1979 or Garay et al. 1993). The population of H II regions of various densities is described by a power-law distribution function, $N(n_e) \propto n_e^{\beta}$, which is normalized by the observed line flux density. The distribution function for galactic diffuse H II regions is a power law (Kennicutt, Edgar, & Hodge 1989). Comeron & Torra (1996) found evidence for a power-law luminosity function for galactic ultracompact H II regions, although Casassus et al. (2000) claim a peaked distribution function. The actual form of the distribution would depend in detail on the star formation history of the starburst region as well as on the evolution of the H II regions. In the model, we use β as a free parameter. The fourth free parameter in Model IV is $n_e^{\min}$, the minimum density in a given distribution.

The observed data was modeled using models I through IV. Valid solutions are identified as those combinations of free parameters that produce both the observed H92α line as well as free-free emission at 4.8, 8.3, and 15 GHz less than the corresponding total observed continuum flux densities (which would include both thermal and nonthermal components). The gas mass and the ionizing photon flux were also derived for each valid solution. All solutions were computed for $T_e = 10{,}000$ and 12,500 K. These high temperatures have been derived from optical spectroscopy and are consistent with the low metallicity of these two galaxies (Campbell et al. 1986; Walsh & Roy 1989; Kobulnicky et al. 1997). Model results for the two galaxies are summarized in Tables 3 and 4. Since Models I and II give similar results, they are grouped together. The allowed range of values of densities and sizes of ionized gas are listed. The range of densities and sizes allowed by the models are quite limited. The gas properties for the models with the minimum allowed value of $N_{\rm Lyc}$ are given in the lower half of Tables 3 and 4. The significance of the minimum allowed $N_{\rm Lyc}$ is as follows: for an arbitrary continuum optical depth τ_c, $N_{\rm Lyc} \propto S_{\rm ff}[\tau_c/(1 - e^{-\tau_c})]$, where $S_{\rm ff}$ is the free-free radio continuum flux density. Hence, for an observed value of $S_{\rm ff}$, the calculated value of the required ionizing photon flux $N_{\rm Lyc}$ increases with increasing continuum optical depth, τ_c. A given value of $S_{\rm ff}$ thus implies a lower limit to the value of $N_{\rm Lyc}$. We take the minimum consistent $N_{\rm Lyc}$ corresponding to the minimum consistent τ_c for modeling. The values for the derived parameters given in Tables 3 and 4 correspond to the average of the range of values allowed by the n_e-l solutions. There are two classes of models allowed by the existing data: $n_e < 2500$ cm^{-3}, $l \sim 5$ pc and $n_e > 2500$ cm^{-3}, $l \sim 30$ pc. The model solutions are indicated in separate rows for each class of solutions. The predictions of some of the valid models for the free-free continuum and line flux densities as a function of frequency are shown in Figure 3. The calculated values of the free-free continuum flux densities are less than the observed total continuum flux densities (which are marked as stars in the figure). The remaining continuum emission that is unaccounted for in our models will have contributions both from thermal con-

TABLE 3

THE LOW-RESOLUTION MODEL RESULTS FOR NGC 5253

Parameter	Models I and II	Model III	Model IV
n_e (cm^{-3})[a]	500–1000 5000–10^4	5000–10^4	2500–25000
Size (pc)[a,b]	20–30 2–7	5–10	3–7
EM (pc cm^{-6})[a]	2×10^7 2×10^8	10^7–10^8	$\sim 10^8$
$M_{\rm H\,II}$ ($M_\odot$)[a]	10^5 10^4	10^4	10^4
Solutions for Minimum $N_{\rm Lyc}$			
$N_{\rm Lyc}^{\rm min}$ (s^{-1})	1.5×10^{52}	2.5×10^{52}	3.5×10^{52}
n_e (cm^{-3})	5000–10^4	5000–10^4	5000–10^4
Size (pc)[b]	2–7	4–7	3–7
EM (pc cm^{-6})	2×10^8	$\sim 10^8$	$\sim 10^8$
$S_{\rm th}/S_{\rm obs}^{\rm cont}$	0.3–0.5	~ 0.7	0.3–0.5
$M_{\rm H\,II}$ ($M_\odot$)	10^4	10^4	5000–10^4
Number of O stars[c]	1100	1825	2600
Mass of stars ($M_\odot$)[d]	2×10^5	3.5×10^5	5×10^5

[a] The two rows correspond to two classes of models, both of which are consistent with existing observations. The models predict different RRL and continuum flux densities at other frequencies (see Fig. 3).

[b] "Effective" sizes are quoted for Models III and IV, i.e., $N_{\rm H\,II}^{1/3} \times l$, where there are $N_{\rm H\,II}$ H II regions of size l.

[c] O3–O9.

[d] Assuming a Salpeter IMF, $m_{\rm upper} = 80\,M_\odot$ and $m_{\rm lower} = 1.0\,M_\odot$.

tinuum from any non–RRL-emitting gas and from the nonthermal continuum (the latter, only in the case of He 2-10, since NGC 5253 has very little contribution from nonthermal emission in the central region). If a significant amount of such a non–RRL-emitting thermal gas is present, the amount of such gas will be strongly constrained by the continuum flux densities at $\nu < 1$ GHz. All the above models will be referred to as "low-resolution" models since these models are based on data with a resolution of 5″, corresponding to a linear size of 150 pc for NGC 5253 and 315 pc for He 2-10. In all four models, the favored parameters are densities of $n_e \sim 10^4$ cm^{-3}, effective sizes of 3–8 pc, and masses of ionized gas of $\sim 10^4\,M_\odot$.

Tables 3 and 4 show that for both the galaxies, the four models give results that are consistent. But, the minimum value of $N_{\rm Lyc}$ varies slightly among the various models. This variation is due to the different geometries assumed in the models and illustrates the uncertainties associated with modeling data with a limited angular resolution. In § 4, we discuss the implications of these results of the low-resolution models.

3.1. *Model IV and the Single-Density Approximation*

As is well known, radio recombination line formation is a non-LTE process. This property can be used to derive densities from observations if the geometry is known. From the theory of RRLs, it is known that a particular recombination line is most efficiently emitted from gas at a particular density and that gas at lower densities emits RRLs preferentially at lower frequencies and vice versa (Zhao et al. 1996). This property of RRLs (as density filters) implies that a particular recombination line would receive maximum contributions from a restricted range of gas densities. Hence, previous work that modeled single-RRL data using the single-density approximation (corresponding to Models I, II, and III in this work) were reasonably successful (Anantharamaiah et al. 1993; Zhao et al. 1996, 1997; Phookun et al. 1998; Anantharamaiah et al. 2000). Therefore, with multifrequency RRL data, the gas can be modeled as a combination of a minimum number of distinct density components. This method was successfully employed to

TABLE 4

THE LOW-RESOLUTION MODEL RESULTS FOR He 2-10

Parameter	Models I and II	Model III	Model IV
n_e (cm^{-3})[a]	500–1000 5000–10^4	5000–50000	2500–25000
Size (pc)[a,b]	30–40 3–8	2–10	2–10
EM (pc cm^{-6})[a]	2×10^7 $\geq 5 \times 10^8$	5×10^7 to 2×10^9	$\sim 10^8$
$M_{\rm H\,II}$ ($M_\odot$)	3×10^5 $\sim 10^4$	7000–40000	10^4
Solutions for Minimum $N_{\rm Lyc}$			
$N_{\rm Lyc}^{\rm min}$ (s^{-1})	2.5×10^{52}	4×10^{52}	5×10^{52}
n_e (cm^{-3})	5000–10^4	5000–50000	5000–10^4
Size (pc)[b]	4–7	5–10	3–7
EM (pc cm^{-6})	$\geq 5 \times 10^8$	$\sim 10^8$	3×10^8
$S_{\rm th}/S_{\rm obs}^{\rm cont}$	0.2–0.5	0.3–0.7	0.3–0.6
$M_{\rm H\,II}$ ($M_\odot$)	$\sim 10^4$	2×10^4	10^4–50000
Number of O stars[c]	1825	2900	3650
Mass of stars ($M_\odot$)[d]	3.5×10^5	5.5×10^5	7×10^5

[a] The two rows correspond to two classes of models, both of which are consistent with existing observations. The models predict different RRL and continuum flux densities at other frequencies (see Fig. 3).

[b] "Effective" sizes are quoted for Models III and IV, i.e., $N_{\rm H\,II}^{1/3} \times l$, where there are $N_{\rm H\,II}$ H II regions of size l.

[c] O3–O9.

[d] Assuming a Salpeter IMF, $m_{\rm upper} = 80\,M_\odot$ and $m_{\rm lower} = 1.0\,M_\odot$.

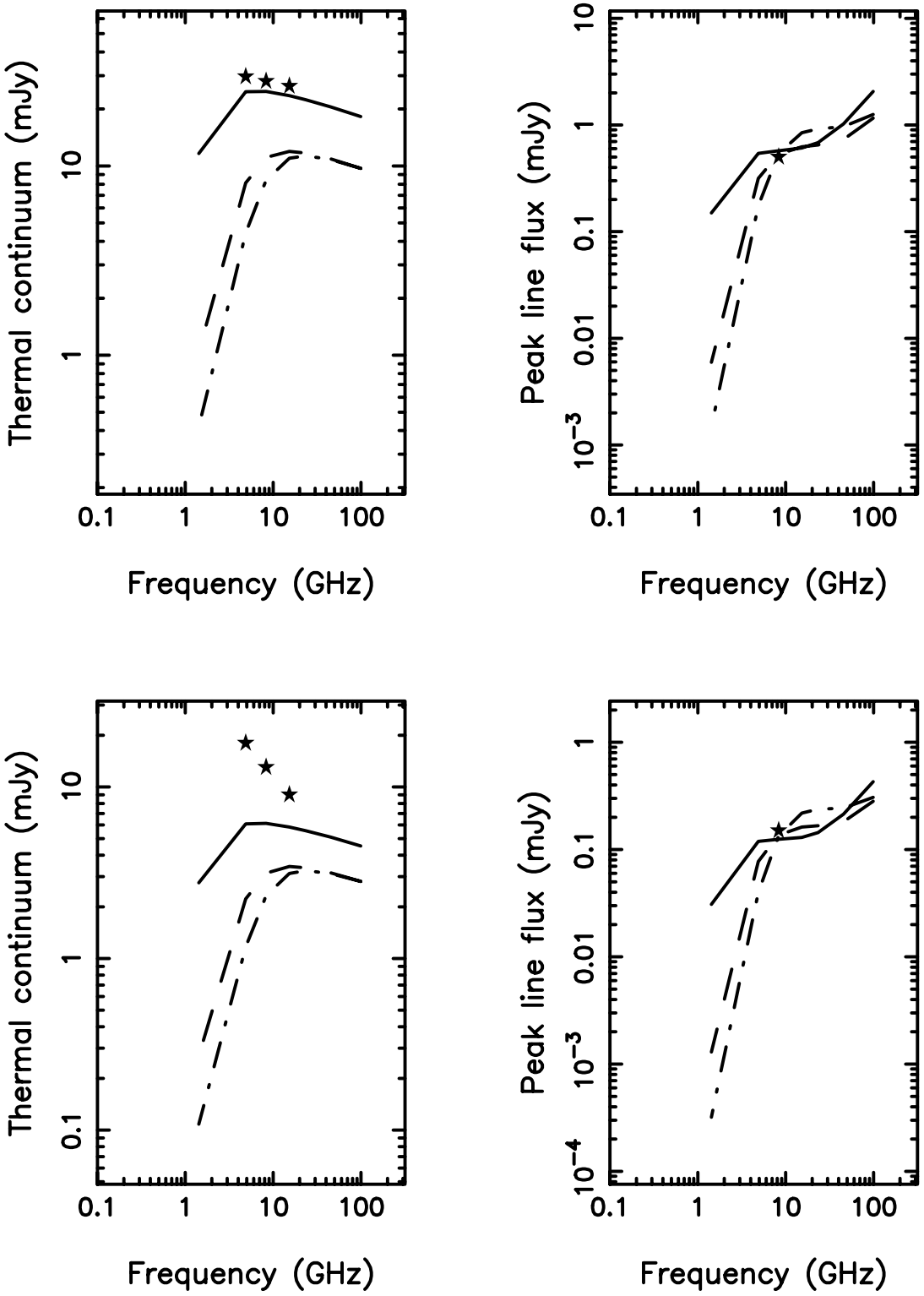

FIG. 3.—Predictions for the thermal continuum and the peak RRL flux densities as a function of frequency for NGC 5253 (*top*) and He 2-10 (*bottom*) for a few valid solutions corresponding to Model I (see § 3 for details). The data points are marked as stars. The solid line corresponds to $n_e = 10^3$ cm^{-3}, $l = 24$ pc, $T_e = 10{,}000$ K, the dashed line to $n_e = 5000$ cm^{-3}, $l = 6$ pc, $T_e = 10{,}000$ K, and the dot-dashed line to $n_e = 10^4$ cm^{-3}, $l = 4$ pc, $T_e = 10{,}000$ K. The predictions of Models II–IV are similar.

derive a three–density component model of the ionized gas in Arp 220 based on line and continuum data from 1.4 to 230 GHz (Anantharamaiah et al. 2000).

However, the single-density approximation based on the above argument is valid only for certain functional dependences of emission measure on density (i.e., on the relative values of emission measures for gas at different densities: the line flux density is most strongly peaked as a function of density when $\beta + 2 + 3/\alpha = 0$; for the line intensity, the condition is $\beta + 2 + 1/\alpha = 0$; see § 3 for definitions of α and

β). For example, Figure 4*a* shows the dependence of the expected line intensity at 8.3 GHz as a function of density, for a constant EM, and the line strength does indeed have a peak as a function of electron density. On the other hand, if a statistically well-sampled population of H II regions with a power-law distribution of EMs with density (as in Model IV) is assumed, the line strength no longer peaks for a particular density but instead is a monotonic function of density. For example, it can be seen in Figure 4*b* that when $N_{\rm Lyc}$ is held constant (i.e., EM $\propto n_e^{4/3}$), the line intensity is no longer a peaked function of density. The results of Model IV show that solutions exist only for values of $n_e^{\rm min}$ ranging between 2500 and 25,000 cm^{-3}. Also, the solutions with the minimum values of $N_{\rm Lyc}$ (the minimum value of $N_{\rm Lyc}$ that is consistent with the given data, corresponding to the minimum needed continuum optical depth; see § 3 for an explanation) correspond to densities between 5000 and 10,000 cm^{-3}. Though no upper limit to the density is imposed on the models, the nature of the allowed solutions is such that only gas of densities very close to $n_e^{\rm min}$ contributes to the line flux density and also absorbs almost all of the required ionizing UV photons; i.e., all the higher density gas in the distribution contributes negligible amounts of RRL emission. This result is common to all valid solutions in this model. We find that the allowed combinations of the free parameters α and $l_{\rm min}$ (the latter being derived from $n_e^{\rm min}$ and c_1; see § 3) are such that the value of $n_e^{\rm min}$ is about 10^4 cm^{-3} and the size of the gas at this density (which is the dominant contributor to the total line strength) is between 3 and 10 pc. This result explains why the results of Models I, II, and III agree well with those of Model IV. Hence, Model IV, which is the first attempt at a consistent multidensity model for extragalactic RRL data, validates the assumption of a single-density ionized gas in modeling the line emission. It should be noted that the narrow range of allowed densities near $\sim 10^4$ cm^{-3} is not the density at which the H92α-line emission is expected to peak (from Fig. 4*a*, this density is $\sim 10^2$ cm^{-3}). That both the constant density models as well as the multiple density models give the same density of $\sim 10^4$ cm^{-3}, vastly different from the density at which H92α is expected to peak, is reason enough to believe that most of the ionized gas in this region does indeed have a density close to 10^4 cm^{-3} and that the amount of gas at a density of 10^2 cm^{-3} must be insignificant compared to the higher density gas.

However, the above argument works only if the density distribution is a power law. In general in a multidensity environment, where the total EM of gas of a given density is an arbitrary function of density, an approach based on Model IV will not work. In such a case, multifrequency

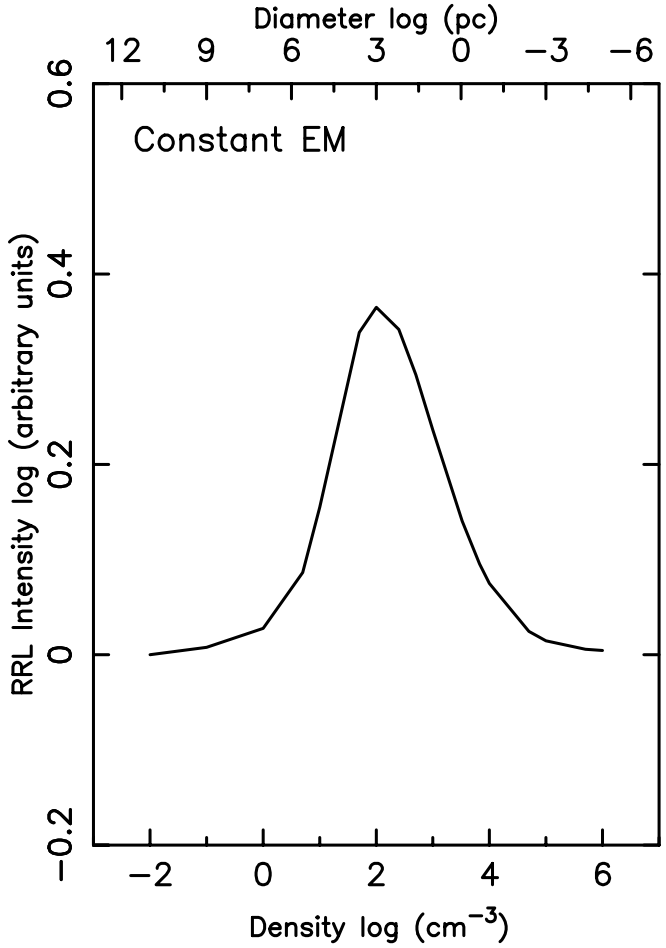

Fig. 4*a*

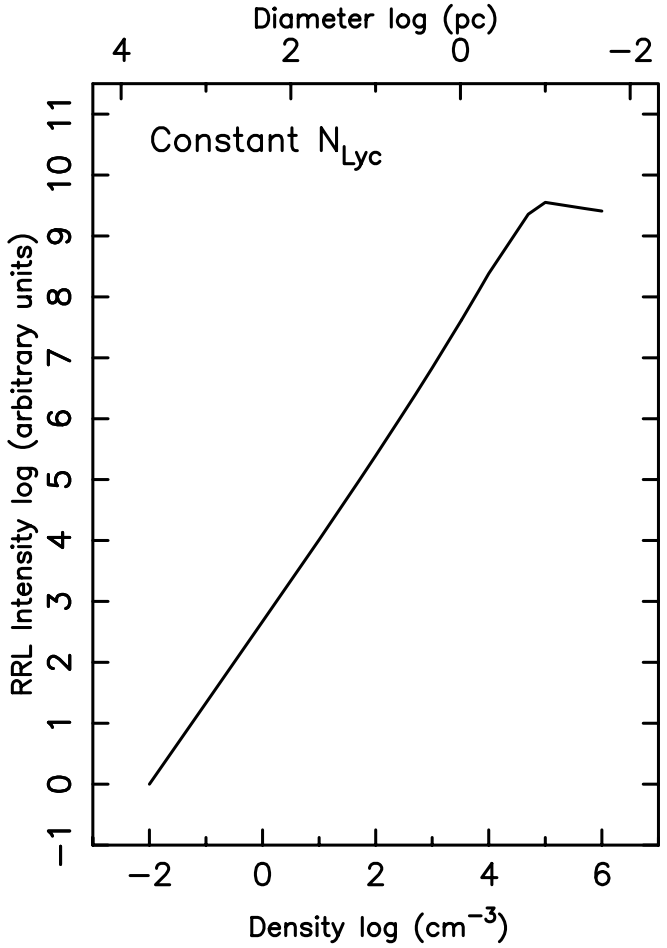

Fig. 4*b*

FIG. 4.—Expected H92α intensity as a function of density for (*a*) constant EM = 10^7 pc cm^{-6} and (*b*) constant $N_{\rm Lyc} = 3 \times 10^{43}$ s^{-1}. Pressure broadening is neglected and non-LTE effects are taken into account. The curve for constant $N_{\rm Lyc}$ illustrates the point that for an arbitrary population of multidensity ionized gas, the RRL strength as a function of density need not a have a maximum over a restricted range of densities.

RRL data is essential and models have to be constructed to explain the data with a minimum number of different density components (as was done in the case of Arp 220 by Anantharamaiah et al. 2000).

4. RESULTS FROM THE LOW-RESOLUTION RADIO RECOMBINATION LINE DATA

4.1. *NGC 5253*

Most of the models discussed in the previous section yield electron densities in excess of a few 1000 cm^{-3} within an effective size of 2-10 pc (Tables 3 and 4). The minimum value of the derived N_{Lyc} is 2.5×10^{52} s^{-1}. This value of N_{Lyc} is computed from the low-resolution data and is consistent with the ionizing photon flux computed from other nebular diagnostics listed below. The continuum flux density of 28 mJy measured from the line-emitting region (which is the position of the peak continuum emission, corresponding to the $6''.5 \times 3''.3$–sized resolution element) in the 8.3 GHz continuum image (Table 2) corresponds to $N_{Lyc} = 3 \times 10^{52}$ s^{-1}, based on the assumption of an optically thin gas. The Hα flux density inside an aperture of 5″ (measured using the Hα image of CMB97) gives an N_{Lyc} of 1.0×10^{52} s^{-1}. The Brγ flux from the central 5″ region (Davies et al. 1998) implies an N_{Lyc} of 1.5×10^{52} s^{-1}, whereas, based on the extinction-corrected Brγ emission strength from the inner $10'' \times 21''$ obtained by Kawara, Nishida, & Phillips (1989), the derived value of N_{Lyc} is 4.5×10^{52} s^{-1}. Within the central $\sim 0''.5$ region, Crowther et al. (1999) have estimated the ionizing photon flux to be 1.1×10^{52} s^{-1}. Although the estimated N_{Lyc} shows evidence of increase with increasing aperture size, the presence of a very patchy dust distribution in NGC 5253 (Gorjian 1996; CMB97) makes it difficult to derive the spatial distribution of the near-IR line emitting ionized gas. In the presence of patchy distribution of dust, the extinctions estimated using data at various wavebands will not match (Natta & Panagia 1984; Israel & Kennicutt 1980), and hence correcting the observed emission strengths for dust absorption is difficult. For this reason, we do not attempt to derive a value for extinction using a comparison of our radio data with the observed Brγ emission. Taking the average value of $N_{Lyc} = 2.5 \times 10^{52}$ s^{-1} and using a Salpeter initial mass function (IMF) with $m_{upper} = 80\ M_\odot$ and the tables given in Vacca, Garmany, & Shull (1996), the number of O stars (O3–O9) is estimated to be ~ 1800. It should be noted that we have used the numbers from Vacca et al. (1996) for solar metallicity, whereas the two galaxies NGC 5253 and He 2-10 have subsolar metallicities; therefore, the calculated values of N_{Lyc} will be underestimated. However, this error is less than 20% (Vacca 1994). Assuming m_{lower} to be $1.0\ M_\odot$, the total number of stars within a region of size ~ 5 pc is $\sim 3.5 \times 10^5$. This ~ 5 pc–sized region of gas could be spread over an entire resolution element (150 pc for NGC 5253). On the other hand, if the gas is physically in a compact region of size ~ 5 pc, then the corresponding stellar density indicates that the ionizing sources may well be SSCs (Meurer et al. 1995).

4.2. *He 2-10*

Similar to the results for NGC 5253, most models for He 2-10 yield electron densities in excess of a few 1000 cm^{-3} within an effective size of 2–10 pc (Table 4). Gas densities of 1000 cm^{-3} have been derived in the central 2″ region using [S II] line ratios (Sugai & Taniguchi 1992). The minimum derived value of N_{Lyc} for the 5″-sized RRL-emitting region is 4×10^{52} s^{-1}. The central 2″ region has been resolved into a number of star-forming knots, and the value of N_{Lyc} derived from observations that resolve these knots is comparable to that derived here. For example, Johnson et al. (2000) obtain a value of $N_{Lyc} = 2.5 \times 10^{52}$ s^{-1} from their UV continuum images. Doyon, Puxley, & Joseph (1992) derive a value of 4×10^{52} s^{-1} from their measured Brγ flux inside a 5″ aperture, which compares well with the value of 3×10^{52} s^{-1} estimated from the Brγ flux density measured inside an aperture of $7'' \times 3''.5$ (Kawara et al. 1989). For an N_{Lyc} of 4×10^{52} s^{-1}, the number of O stars required is ~ 2900 and the total stellar mass is $\sim 5.5 \times 10^5\ M_\odot$ (using a Salpeter IMF with $m_{upper} = 80\ M_\odot$, $m_{lower} = 1.0\ M_\odot$ and the results of Vacca et al. 1996). As in the case of NGC 5253, the corresponding stellar density for a 3–10 pc region corresponds to an SSC, if we assume that the ionized gas is physically confined to this ~ 5 pc region (see § 5.2 for more details).

Though the derived ionizing photon flux and the length scale of the gas for both galaxies imply an SSC, the 8.3 GHz RRL data alone does not clarify whether the ionized gas is in a single clump of diameter ~ 5 pc or is spread out in some unknown geometry over the entire 5″ region. In the latter case, the ionizing source need not be an SSC. In the next section, we present arguments that the ionized gas is indeed much less than 5″ in size. We also discuss the implications of combining our RRL data and model results with recently published subarcsecond resolution continuum images of the centers of the two galaxies (obtained by TBH00 for NGC 5253 and by KJ99 for He 2-10).

5. COMPACTNESS OF THE RADIO RECOMBINATION LINE EMISSION: EVIDENCE FROM OTHER HIGH-RESOLUTION OBSERVATIONS

5.1. *NGC 5253*

We can indirectly infer that the RRL-emitting region is smaller than 5″ from the Hα and Hβ images of CMB97. The Hα image in the inner 5″ is quite clumpy with extensive filaments and knots. Though the RRL emission need not follow the Hα emission, it is unlikely that the high-density gas responsible for RRL emission is spread smoothly over the 150 pc region, given the patchy appearance of the Hα emission, and hence we may conclude that the RRL-emitting gas must also be patchy within the 5″ beam.

TBH00 have imaged NGC 5253 at 23 and 15 GHz with the VLA with angular resolutions of 0″.13 and 0″.2, respectively. A compact ($\sim 0''.1$, or 2 pc) source with a flux density of 11 mJy at 15 GHz, and hence a brightness temperature of $12{,}000 \pm 3000$ K, was discovered. This was interpreted as an H II region, and in addition, these authors detect radio emission at a low level with a size of 1″–2″. Further confirmation of the thermal nature of this source comes from recently detected IR emission from the central object at 11.7 and 18.7 μm (Gorjian, Turner, & Beck 2001). Though the RRL emission is not expected to exactly follow the morphology of continuum emission (since a particular RRL comes from a limited range of densities and the continuum emission is sensitive to all densities if optically thin), no line emission is expected from continuum-free regions, and hence we can associate the observed H92α emission with the inner 1″–2″ region. Assuming that the observed radio con-

tinuum emission from this galaxy is purely due to free-free emission, TBH00 derive an rms electron density of 4×10^4 cm^{-3} and an $N_{\rm Lyc}$ of 4×10^{52} s^{-1}. From the ionization requirement and the size of the object, TBH00 suggest that this compact source is a supernebula surrounding an SSC. Since this source is the strongest radio continuum source in the inner 5″ region and since the derived properties of the supernebula, especially the local electron density, match those derived from the RRL data, we tentatively identify the RRL-emitting gas with the continuum source detected by TBH00. Therefore, we have modeled the supernebula to estimate the fraction of the observed RRL emission that this compact source is capable of producing. The models are constructed to produce the observed 11 mJy continuum emission at 15 GHz from gas of size $\sim$0.″1. In addition, the continuum and RRL emission by this gas at 8.3 GHz is also constrained to be less than the observed values (the latter two constraints are imposed as upper limits since the observed values correspond to the larger 5″ area). The results of this model are summarized in Table 5. Only 10%–35% of the observed 8.3 GHz–line emission can be explained by the TBH00 supernebula. All densities $\geq 5 \times 10^4$ cm^{-3} are consistent with the existing observations. The remaining line emission presumably originates in the surrounding larger nebulosity with a size of 1″–2″. A calculation similar to the one above, where we model the inner 3″ region with a 15 GHz flux density of 22 mJy (TBH00), shows that such a model is indeed capable of explaining the entire observed RRL emission.

The supernebula as imaged by TBH00 is separated by about 0.″9 from the position of the brightest Hα knot in CMB97. This knot was identified with the UV cluster 5 in the *HST* image by Meurer et al. (1995). Since the 1 σ error between the absolute reference frames of the Guide Star Catalogue 1 of the *HST*, on which the Hα and UV images are based, and the extragalactic radio reference frame, on which the images in TBH00 are based, is 0.″5 (Russell et al. 1990 and also D. Calzetti, 2001, private communication, and J. Rajagopal 2001, private communication), the radio supernebula of TBH00 can also be identified with the Hα peak (and hence the UV cluster 5) within these errors. The significance of this identification is twofold: (1) an additional highly obscured SSC need not be invoked, and (2) we can relate the known properties of the optical cluster with those of the supernebula. The Hα flux for this cluster is 4.8×10^{-16} W m^{-2} (see CMB97), from which we infer the value of $N_{\rm Lyc}$ to be $\sim 1.3 \times 10^{51}$ s^{-1}. The discrepancy between this value and $N_{\rm Lyc} > 2.5 \times 10^{52}$ s^{-1}, which is derived from radio continuum data (Table 5), can be attributed to extinction. However, as the age of the optical cluster is well constrained, the dynamical age of the ionized supernebula around it can also be constrained (see § 7.1 for further details).

TABLE 5

MODEL RESULTS FOR 8.3 GHz LINE AND THE HIGH-RESOLUTION CONTINUUM DATA OF KJ99 AND TBH00

Parameter	NGC 5253	He 2-10
n_e (cm^{-3})	5×10^4 to 1×10^6	5000–10000
Size (pc)	1.0–2	$\sim$7
$N_{\rm Lyc}$ (s^{-1})	$>(2.5\text{–}4.0) \times 10^{52}$[a]	$>2.5 \times 10^{52}$
τ_c	≥ 10	$\sim$0.6
$(S_{\rm H92\alpha})_{\rm model}/(S_{\rm H92\alpha})_{\rm obs}$	0.1–0.35	$\sim$1
$M_{\rm H\,II}$ ($M_\odot$)	$\geq$2000	$\geq 2 \times 10^4$
Number of O stars[b]	>1900–2900	>1900
Mass of stars ($M_\odot$)[c]	$>(3.5\text{–}5.5) \times 10^5$	$>3.5 \times 10^5$

[a] The range 2.5–4 is over various models.
[b] O3–O9.
[c] Assuming a Salpeter IMF with $m_{\rm upper} = 80\ M_\odot$ and $m_{\rm lower} = 1.0\ M_\odot$.

5.2. *He 2-10*

The central 5″ region harbors about nine UV clusters, possibly SSCs, arranged in an arc of size $\sim$2″ (Conti & Vacca 1994). This region has a large patchy extinction and also clumpy ionized gas. The Brγ, UV, and optical continuum images of the center show the presence of several knots (Davies et al. 1998; Conti & Vacca 1994; Johnson et al. 2000). KJ99 have imaged the radio continuum emission of the nucleus of He 2-10 with an angular resolution of 0.″5 using the VLA. They detect four to five compact knots, each of diameter $\sim$0.″6, arranged within a 5″ × 2″ region. These knots of star formation detected individually in the optical, Hα, Brγ, and radio continuum are not positionally consistent, possibly due to intrinsic astrometric errors. Attempts at aligning the various images using global astrometric offset corrections have shown that not all knots have counterparts at all wavelengths (KJ99 and Johnson et al. 2000); thus, there appears to be hidden regions of star formation in the central 5″ region. This morphological evidence for the clumpy gas at the center indicates that the RRL-emitting gas is also clumpy on scales $<5''$.

Based on the continuum spectra, KJ99 infer that the radio knots consist of thermal gas at densities 1500–5000 cm^{-3} (optically thick at 8.3 GHz) and also derive a total $N_{\rm Lyc}$ of 4×10^{52} s^{-1}. They suggest that each compact knot may be ionized by an SSC. We have modeled this region to look for solutions that produce the observed radio continuum flux densities at 15, 8, and 5 GHz, as reported by KJ99. The allowed solutions are also constrained to produce either all or a part of the observed H92α line. The model results are listed in Table 5, and these radio knots, if thermal, are indeed capable of producing all of the observed H92α recombination line. Therefore, we identify these multiple radio continuum knots with the gas responsible for emitting the observed RRL at 8.3 GHz and associate the ionizing sources with SSCs.

6. NGC 5253 AND RADIO–FAR-INFRARED CORRELATION

The far-IR (FIR) luminosity and the radio luminosity of galaxies that are dominated by star formation, as opposed to an active galactic nucleus, are very tightly correlated, with an rms of $\leq$0.2 dex on the logarithmic scale (Condon 1992). This radio-FIR correlation holds for several types of galaxies, such as normal spirals, dwarf starbursts, and dwarf irregulars (see Condon 1992). The physical reason for this correlation is not well understood in detail but may result from a chain of events involving star formation. The thermal (free-free) portion of the radio emission is from gas ionized by OB stars, and the nonthermal (synchrotron) portion of the radio emission arises from the cosmic rays accelerated in SNRs, the endpoint of Type II SNe caused by massive stars. The warm ($T > 30$ K, $S_{60\mu{\rm m}}/S_{100\mu{\rm m}} \geq 1$) dust portion of the FIR emission arises from dust directly heated by OB stars, and the cool ($T < 30$ K, $S_{60\mu{\rm m}}/S_{100\mu{\rm m}} < 0.8$) dust portion of the FIR emission arises from dust heated by the diffuse interstellar radiation field. Xu et al. (1992) have

shown in the case of the LMC that the warm dust emission correlates with the thermal radio emission, while the cool dust emission correlates independently with the nonthermal radio emission. Also, the ratio of the two correlated quantities for both these independent correlations was shown to be the same as that between the total FIR and the total radio emission strengths.

The radio continuum of most disk galaxies is dominated by nonthermal emission since the thermal fraction is typically 0.05–0.2 at 1.4 GHz (Condon 1992). But, it is known that the BCDGs have a higher fraction of thermal emission than disk galaxies: Klein & Wunderlich (1987) showed that the average radio spectral index $\langle\alpha\rangle$ is -0.4 for BCDGs, while it is -0.7 for normal spirals, $S_\nu \propto \nu^\alpha$. Though the mean spectral index is indeed flatter for BCDGs, the dispersion in the index is much larger than for spirals, and hence they did not estimate an average thermal fraction for the BCD galaxy sample. BCDGs also have a higher dust temperature (Wunderlich & Klein 1988, hereafter WK88) compared to spiral galaxies, which implies that their FIR emission is dominated by emission from warm dust. It has been suggested by Klein & Wunderlich (1987) and WK88 that the reason the BCDGs also obey the radio-FIR correlation is because this dominant warm dust emission correlates with the thermal radio emission, which is the dominant portion of the radio continuum.

NGC 5253 may well be a unique case that will help to understand the details of the radio-FIR correlation. Radio continuum flux density measurements at various frequencies using single dishes and low-resolution images have shown that the radio emission of NGC 5253 is consistent with being almost purely thermal (see Beck et al. 1996 and also the spectral index map of Turner et al. 1998). Its total flux density at 1.4 GHz is 89 mJy (from the NRAO VLA Sky Survey catalog of Condon et al. 1998 and single-dish observations), and the FIR flux is calculated to be 8×10^8 $L_\odot$ from the *IRAS* flux densities. From the ratio of the radio to the FIR luminosity, it can be seen that this galaxy obeys the radio-FIR correlation (Condon 1992) to within 1.5 σ. This is a surprising result, since the nonthermal emission in this galaxy is less than 10% of the total emission at 5 GHz (Beck et al. 1996; Turner et al. 1998). It is known that the radio flux density and the FIR flux density of galactic H II regions are also correlated, but with a different ratio (Wynn-Williams & Becklin 1974; Fuerst, Reich, & Sofue 1987; Broadbent, Osborne, & Haslam 1989). On the other hand, the ratio of radio to FIR flux densities of compact H II regions is not a constant but depends on a variety of factors (Kurtz, Churchwell, & Wood 1994). It is worth noting that though the radio emission of NGC 5253 is almost purely thermal, the radio-to-FIR emission ratio is similar to that of star-forming galaxies rather than that of H II regions. One way to explain the correlation is the following: the dust temperature in the nucleus of NGC 5253 is high (Calzetti et al. 1995 estimated it to be 51 K). This high dust temperature is the reason why the ratio of the strength of the warm dust emission to the cool dust emission is about 16, one of the largest among BCDGs and disk galaxies (Calzetti et al. 1995). Therefore, we suggest that the reason NGC 5253 obeys the radio-FIR correlation is that the warm dust emission and the thermal radio emission are indeed correlated with each other, and the slope of the correlation is the same as that between the total FIR and total radio in normal spirals, as suggested by Xu et al. (1992) and WK88. WK88 had also put forward an alternative explanation for BCDGs obeying the radio-FIR correlation: they had suggested that a possible lower dust fraction in these galaxies would compensate for the lower nonthermal radio fraction. This explanation is unlikely for NGC 5253, since among all BCDGs, it has the lowest nonthermal fraction but the highest dust-to-gas ratio (Lisenfeld & Ferrara 1998).

7. DISCUSSION

The detection of an RRL from the central region of both galaxies with parameters similar to those derived by TBH00 and KJ99 is added confirmation for the thermal nature of the central compact source(s). Additionally, an RRL study of dense ionized gas has the following advantages : (1) Instead of the rms electron density as given by the continuum data, local electron densities, independent of filling factor, can be derived from RRL data. (2) Therefore, if the line-emitting region is spatially resolved, then the actual value of $N_{\rm Lyc}$ can be derived (and not just the lower limit). (3) Because of non-LTE effects, RRLs retain their sensitivity to density even in gas that is moderately optically thick, unlike continuum emission.

7.1. *Dynamics of Ionized Gas around SSCs*

A question not yet addressed regards the dynamics and timescales involved in explaining the existence of $\sim 10^4$ $M_\odot$ of ionized gas within a few parsecs of an SSC. In this section, we will identify the supernebula(e) with the RRL-emitting gas in both the galaxies and also tentatively associate the supernebula in NGC 5253 with the star cluster in the center. The observed FWHM of ~ 100 km s^{-1} (estimated from the spectrum before off-line Hanning smoothing) within a 2–8 pc sized region implies a dynamical expansion time of (2–8) $\times 10^4$ yr, quite short compared to the estimated age of (1–3) $\times 10^6$ yr for the central cluster in NGC 5253. Therefore, either the supernebula must have been set in motion extremely recently or there must exist a confining mechanism operating in the central region. In addition, strong stellar winds from OB and Wolf-Rayet stars as well as the natural expansion of the H II region due to overpressure would drive the ionized gas outward. Given the large mass, high density, and small size of the observed H II region (~ 2 pc for the supernebula of TBH00 and KJ99 and 5–8 pc for the RRL-emitting gas), dynamical models should constrain both the age of the SSC as well as the density of the ambient unshocked medium. For NGC 5253, for example, if the supernebula is identified with the UV cluster 5, then the age is determined to be less than 3 million yr (CMB97).

If we assume the H II region to have reached a diameter of 1 pc solely due to expansion driven by overpressure in ~ 2 Myr, then the radius of the initial Stromgren sphere would be ~ 0.01 pc (Spitzer 1968). If at the time of formation of the initial Stromgren sphere the ionizing photon flux were $\sim 10^{52}$ s^{-1}, then the corresponding initial density should be $\sim 2 \times 10^7$ cm^{-3}. In such a case, the mass of the shocked neutral gas between the shock and the ionization fronts would be more than 100 times greater in the ionized gas inside the ionization front (Savedoff & Greene 1955).

In addition, stellar winds will definitely play an important dynamical role. Using StarBurst 99 (Leitherer et al. 1999), a mechanical luminosity of 10^{38} ergs s^{-1} is estimated for an $N_{\rm Lyc}$ of 10^{52} s^{-1}, assuming a continuous starburst model.

Assuming that the isothermal phase sets in early in the lifetime of the H II region, the radius of the thin swept-up ionized shell is given by $R_{\rm iso} = 16(L/n_0\,V)^{1/4}t_6^{1/2}$ pc, where L is the mechanical luminosity in units of 10^{36} ergs s^{-1}, V is the velocity of the stellar wind at infinity (assumed to be 1000 km s^{-1}), n_0 is the density of the ambient medium, and t_6 is the time in millions of years (McCray 1983). The thickness of the ionized shell is given by $n_0 R_{\rm iso}/3n_s$ (Dyson & Williams 1997), where n_s, the density of the shocked ionized gas, is given by $n_s = n_0(V_s^2/C^2)$ for an isothermal shock (V_s is the velocity of the shock, $dR_{\rm iso}/dt$, and C is the speed of sound in the ambient medium). The values of n_0 and t can be expressed in terms of n_s and the mass of the ionized gas. The ranges of input parameters are 10^3 cm$^{-3} \le n_s \le 5 \times 10^4$ cm^{-3} and $10^3\ M_\odot \le M \le 10^4\ M_\odot$, which are similar to the ranges for the models in Tables 3 and 4. The ranges of the derived values are 0.01 cm$^{-3} \le n_0 \le 100$ cm^{-3} and 10^5 yr $\le t \le 2 \times 10^6$ yr. Although the derived values do not violate any known constraints, the allowed solution space and a detailed modeling based on future higher resolution continuum images would be useful to understand the dynamics and the ambient environment of these regions. For an initial attempt at such an analysis, see Tan & McKee (2001).

7.2. *High-Density Ionized Gas in Starburst Regions*

The commonly occurring relatively high density of $\sim 10^4$ cm^{-3} for the compact ionized gas in the starburst regions in He 2-10 and NGC 5253 and also in other starburst galaxies (Gilbert et al. 2000; Zhao et al. 1997; Anantharamaiah et al. 2000; TBH00; KJ99) is striking. One model that may be able to explain these commonly occurring high densities is that of Jog & Das (1992, 1996). In their model, a giant molecular cloud (GMC) in the center of a starburst region is shocked by the overpressure of the surrounding molecular intercloud medium (ICM). The outer shell of the GMC is shock compressed and moves inward, and at a later stage, due to onset of gravitational instabilities, it fragments into star-forming centers. This model can well explain the formation of SSCs of mass $\ge 10^5\ M_\odot$. An estimate of the density of the shell fragments when star formation begins in the imploding shell is possible. From Jog & Das (1996), the velocity of the shock, V_s, at the onset of gravitational instabilities can be as high as ~ 30 km s^{-1}, and the radius of the shock front reaches $\sim 40\%$ of the GMC radius. Adopting a value of the sound speed, C_s, inside the GMC as 4 km s^{-1}, the density of the shocked gas, $n_s = n_0(V_s^2/C_s^2)$, is increased, and the value of the density enhancement n_s/n_0 can be greater than 55 (this enhancement can be up to 3 times larger than this value, for the observed range of values of GMC and ICM properties). In their model, Jog & Das (1992, 1996) assume that the density of the GMC falls radially as r^{-1} and that the density at the boundary is at least 100 cm^{-3}. Therefore, this density enhancement could explain the observed densities of 10^3–10^4 cm^{-3} observed in RRLs. It remains to be seen if there is indeed a high-pressure reservoir of molecular gas or shocked hot gas at the centers of these galaxies and, if so, whether star formation occurs via this process. It should be noted that CO images of the centers of these two galaxies do not show evidence for gas in this region, and therefore we appeal to whichever gas reservoir gave rise to the SSCs in the center to provide the necessary high pressure. However, the high-density ambient medium is not needed as in the previous cases, since remnant clouds of density $\sim 10^4$ cm^{-3} would still remain in the vicinity of the star cluster and be ionized.

The RRL observations in this paper and the recent continuum observations of supernebulae may well be the first detection of ionized gas around extremely young SSCs. Since these clusters are usually too obscured to be studied even in the IR, higher resolution radio continuum and line data can be used to infer the properties of the ambient medium around SSCs and, ultimately, the formation mechanism of these massive clusters. Sensitive line data will also yield kinematic information about these nebulae. But, an important problem is the identification of the radio components with the optical and UV components at the subarcsecond level, which should be achievable in a few years.

8. SUMMARY

We have detected the H92α recombination line from two dwarf starbursts, NGC 5253 and He 2-10. The ionized gas responsible for both line emission and the radio continuum emission is modeled in terms of electron density and size. The line-emitting gas in both galaxies is found to be of densities $\sim 10^4$ cm^{-3} with a size of 2–10 pc, implying an $N_{\rm Lyc}$ of a few times 10^{52} s^{-1}. We also consider a multi-density model for the RRL-emitting gas and show that the assumption of a constant density in previous models is valid in a wide range of cases. Though the line emission is spatially unresolved and the linear size of the beam area corresponds to 150 and 315 pc, respectively, for NGC 5253 and He 2-10, we present arguments that suggest that the line emission is compact (a few parsecs). Based on the derived parameters, these lines seem to originate from ionized gas associated with SSCs in both galaxies. The possible supernebulae around these clusters have been detected in radio continuum emission, and we show that these nebulae are capable of producing all the observed line emission in both the galaxies.

Both the detection of RRL emission as well as direct radio continuum imaging of these supernebula around SSCs pose problems about the lifetimes and dynamics of the ionized gas. We present simple arguments to show that reconciling the dynamical age of the supernebula with the age of the SSCs might be difficult and that detailed observational data as well as theoretical modeling are necessary in order to understand the dynamics of H II regions around these massive clusters. Finally, we point out that though NGC 5253 has a thermal radio spectrum, it seems to obey the radio-FIR correlation, which is known to hold for galaxies dominated by nonthermal radio emission. This feature may well be evidence for the warm dust portion of the FIR emission to be correlated with the thermal radio emission, independent of the cold dust FIR emission and the nonthermal radio emission, as suggested by Xu et al. (1992).

The National Radio Astronomy Observatory is a facility of the National Science Foundation operated under cooperative agreement by Associated Universities, Inc. This research has made use of the NASA/IPAC Extragalactic Database (NED), which is operated by the Jet Propulsion Laboratory, California Institute of Technology, under contract with the National Aeronautics and Space Administration. We would like to express our appreciation to the Starburst 99 team for having made their code public and also for making it possible to run the code on line. A part of this work was carried out by N. R. M. and K. R. A. at the

National Radio Astronomy Observatory in Socorro, New Mexico, and they thank NRAO for financial support. We thank Daniela Calzetti for the use of her Hα image of NGC 5253, Chanda Jog for discussions, and Dwarakanath for a careful reading of the paper and useful comments. We also thank the referee, J. L. Turner, for useful comments and suggestions. This research has made use of NASA's Astrophysics Data System Abstract Service.

REFERENCES

Allen, D. A., Wright, A. E., & Goss, W. M. 1976, MNRAS, 177, 91
Anantharamaiah, K. R., Viallefond, F., Mohan, N. R., Goss, W. M., & Zhao, J.-H. 2000, ApJ, 537, 613
Anantharamaiah, K. R., Zhao, J.-H., Goss, W. M., & Viallefond, F. 1993, ApJ, 419, 585
Atherton, P. D., Taylor, K., Pike, C. D., Harmer, C. F. W., Parker, N. M., & Hook, R. N. 1982, MNRAS, 201, 661
Beck, S. C., Turner, J. L., Ho, P. T. P., Lacy, J. H., & Kelly, D. 1996, ApJ, 457, 610
Broadbent, A., Osborne, J. L., & Haslam, C. G. T. 1989, MNRAS, 237, 381
Caldwell, N., & Phillips, M. M. 1989, ApJ, 338, 789
Calzetti, D., Bohlin, R. C., Kinney, A. L., Storchi-Bergmann, T., & Heckman, T. M. 1995, ApJ, 443, 136
Calzetti, D., Meurer, G. R., Bohlin, R. C., Garnett, D. R., Kinney, A. L., Leitherer, C., & Storchi-Bergmann, T. 1997, AJ, 114, 1834 (CMB97)
Campbell, A., Terlevich, R., & Melnick, J. 1986, MNRAS, 223, 811
Casassus, S., Bronfman, L., May, J., & Nyman, L.-Å. 2000, A&A, 358, 514
Comeron, F., & Torra, J. 1996, A&A, 314, 776
Condon, J. J. 1992, ARA&A, 30, 575
Condon, J. J., Cotton, W. D., Greisen, E. W., Yin, Q. F., Perley, R. A., Taylor, G. B., & Broderick, J. J. 1998, AJ, 115, 1693
Conti, P. S., & Vacca, W. D. 1994, ApJ, 423, L97
Corbin, M. R., Korista, K. T., & Vacca, W. D. 1993, AJ, 105, 1313
Cornwell, T. J., Uson, J. M., & Haddad, N. 1992, A&A, 258, 583
Crowther, P. A., Beck, S. C., Willis, A. J., Conti, P. S., Morris, P. W., & Sutherland, R. S. 1999, MNRAS, 304, 654
Davies, R. I., Sugai, H., & Ward, M. J. 1998, MNRAS, 295, 43
Doyon, R., Puxley, P. J., & Joseph, R. D. 1992, ApJ, 397, 117
Dyson, J. E., & Williams, D. A. 1997, The Physics of the Interstellar Medium (2d ed.; Bristol: Inst. Physics Publishing)
Fuerst, E., Reich, W., & Sofue, Y. 1987, A&AS, 71, 63
Garay, G., Rodriguez, L. F., Moran, J. M., & Churchwell, E. 1993, ApJ, 418, 368
Gilbert, A. M. 2000, ApJ, 533, L57
Gorjian, V. 1996, AJ, 112, 1886
Gorjian, V., Turner, J. L., & Beck, S. C. 2001, ApJ, 554, L29
Graham, J. A. 1981, PASP, 93, 552
Habing, H. J., & Israel, F. P. 1979, ARA&A, 17, 345
Heckman, T. M., Armus, L., & Miley, G. K. 1990, ApJS, 74, 833
Israel, F. P., & Kennicutt, R. C. 1980, Astrophys. Lett., 21, 1
Jog, C. J., & Das, M. 1992, ApJ, 400, 476
———. 1996, ApJ, 473, 797
Johnson, K. E., Leitherer, C., Vacca, W. D., & Conti, P. S. 2000, AJ, 120, 1273
Kawara, K., Nishida, M., & Phillips, M. M. 1989, ApJ, 337, 230
Kennicutt, R. C., Jr., Edgar, B. K., & Hodge, P. W. 1989, ApJ, 337, 761
Klein, U., & Wunderlich, E. 1987, in Star Formation in Galaxies (NASA CP-2466), 583
Kobulnicky, H. A., Dickey, J. M., Sargent, A. I., Hogg, D. E., & Conti, P. S. 1995, AJ, 110, 116
Kobulnicky, H. A., & Johnson, K. E. 1999, ApJ, 527, 154 (KJ99)
Kobulnicky, H. A., Skillman, E. D., Roy, J.-R., Walsh, J. R., & Rosa, M. R. 1997, ApJ, 477, 679
Kronberg, P. P., Biermann, P., & Schwab, F. R. 1985, ApJ, 291, 693
Kurtz, S., Churchwell, E., & Wood, D. O. S. 1994, ApJS, 91, 659
Leitherer, C., et al. 1999, ApJS, 123, 3
Lequeux, J. 1971, A&A, 15, 30
Lisenfeld, U., & Ferrara, A. 1998, ApJ, 496, 145
McCray, R. 1983, in Highlights of Astronomy, Vol. 6, ed. R. West (Dordrecht: Reidel), 565
Méndez, D. I., Esteban, C., Filipović, M. D., Ehle, M., Haberl, F., Pietsch, W., & Haynes, R. F. 1999, A&A, 349, 801
Meurer, G. R., Heckman, T. M., Leitherer, C., Kinney, A., Robert, C., & Garnett, D. R. 1995, AJ, 110, 2665
Natta, A., & Panagia, N. 1984, ApJ, 287, 228
Neff, S. G., & Ulvestad, J. S. 2000, AJ, 120, 670
Phookun, B., Anantharamaiah, K. R., & Goss, W. M. 1998, MNRAS, 295, 156
Puxley, P. J., Brand, P. W. J. L., Moore, T. J. T., Mountain, C. M., & Nakai, N. 1991, MNRAS, 248, 585
Russell, J. L., Lasker, B. M., McLean, B. J., Sturch, C. R., & Jenkner, H. 1990, AJ, 99, 2059
Saha, A., Sandage, A., Labhardt, L., Schwengeler, H., Tammann, G. A., Panagia, N., & Macchetto, F. D. 1995, ApJ, 438, 8
Savedoff, M. P., & Greene, J. 1955, ApJ, 122, 477
Schaerer, D., Contini, T., Kunth, D., & Meynet, G. 1997, ApJ, 481, L75
Seaquist, E. R., & Bell, M. B. 1977, A&A, 60, L1
Shaver, P. A., Churchwell, E., & Rots, A. H. 1977, A&A, 55, 435
Spitzer, L. 1968, Diffuse Matter in Space (New York: Interscience)
Sugai, H., & Taniguchi, Y. 1992, AJ, 103, 1470
Tan, J. C., & McKee, C. F. 2001, in Starburst Galaxies, Near and Far, ed. D. Lutz & L. Tacconi (Springer Proceedings in Physics 88; New York: Springer), in press (astro-ph/0012005)
Tarchi, A., Neininger, N., Greve, A., Klein, U., Garrington, S. T., Muxlow, T. W. B., Pedlar, A., & Glendenning, B. E. 2000, A&A, 358, 95
Turner, J. L., Beck, S. C., & Ho, P. T. P. 2000, ApJ, 532, L109 (TBH00)
Turner, J. L., Ho, P. T. P., & Beck, S. C. 1998, AJ, 116, 1212
Ulvestad, J. S., & Antonucci, R. J. 1997, ApJ, 488, 621
Vacca, W. D. 1994, ApJ, 421, 140
Vacca, W. D., Garmany, C. D., & Shull, J. M. 1996, ApJ, 460, 914
van den Bergh, S. 1980, PASP, 92, 122
Walsh, J. R., & Roy, J.-R. 1987, ApJ, 319, L57
———. 1989, MNRAS, 239, 297
Whitmore, B. C. 2000, preprint (astro-ph/0012546)
Wunderlich, E., & Klein, U. 1988, A&A, 206, 47 (WK88)
Wynn-Williams, C. G., & Becklin, E. E. 1974, PASP, 86, 5
Xu, C., Klein, U., Meinert, D., Wielebinski, R., & Haynes, R. F. 1992, A&A, 257, 47
Zhao, J.-H., Anantharamaiah, K. R., Goss, W. M., & Viallefond, F. 1996, ApJ, 472, 54
———. 1997, ApJ, 482, 186